Structural Engineering and Mechanics, Vol. 5, No. 3 (1997) 297-306
DOI: http://dx.doi.org/10.12989/sem.1997.5.3.297

Analysis of a cantilever bouncing against a stop according to Timoshenko beam theory

Hsiang-Chuan Tsai† and Ming-Kuen Wu‡

Department of Construction Engineering, National Taiwan Institute of Technology, P.O. Box 90-130, Taipei, Taiwan, R.O.C.

Abstract. The bouncing of a cantilever with the free end pressed against a stop can create high-frequency vibration that the Bernoulli-Euler beam theory is inadequate to solve. An analytic procedure is presented using Timoshenko beam theory to obtain the non-linear response of a cantilever supported by an elastic stop with clearance at the free end. Through a numerical example, the bouncing behavior of the Timoshenko and Bernoulli-Euler beam models are compared and discussed.

Key words: Timoshenko beam; impact; gap; nonlinear vibration.

1. Introduction

Bouncing of dynamic systems against stops is of great concern in many industries. This phenomenon occurs in such cases as the impact of gapped supports on piping systems in nuclear power plants (Salmon, *et al.* 1985, Tsai, *et al.* 1989) and the pounding of adjacent buildings during earthquakes (Maison and Kasai 1990). The bouncing behavior of a system simplified as a cantilever beam with the free end supported by a spring with clearance was extensively investigated (Lo 1980, Masri, *et al.* 1981, Shaw 1985). All these studies employed the Bernoulli-Euler beam theory that takes no account of effects of rotatory inertia and transverse shear deformation. According to experimental data, bouncing of a cantilever can induce high-frequency vibration (Lo 1980, Masri, *et al.* 1981) and the Bernoulli-Euler beam theory is inadequate for the vibration of higher modes (Aprahamian and Evensen 1970). Although the lower modes are of primary interest for usual engineering applications, for some applications, such as wave-propagation studies, it is of interest to investigate high-frequency vibration modes. Theoretical study shows that the use of the Timoshenko beam theory, which takes into account the effects of rotatory inertia and shear deformation, leads to more realistic results in the impact problem (Kelly 1967). The purpose of this present paper is to apply the Timoshenko beam theory to investigate the bouncing behavior of cantilever beams. A non-linear solution scheme using modal analysis to solve the problem of multiple impacts is developed first. Through numerical examples, the calculated responses based on Timoshenko and Bernoulli-Euler beam theories are compared and discussed.

† Professor
‡ Graduate Student

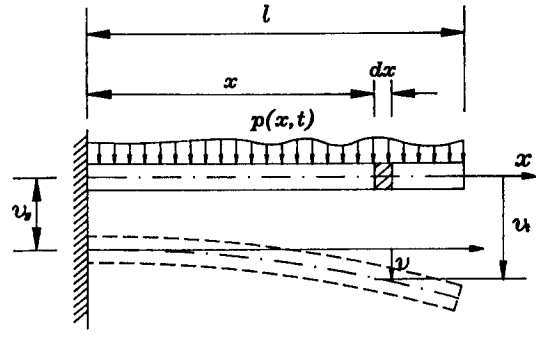

Fig. 1 Cantilever excited by distributed loading and support motion.

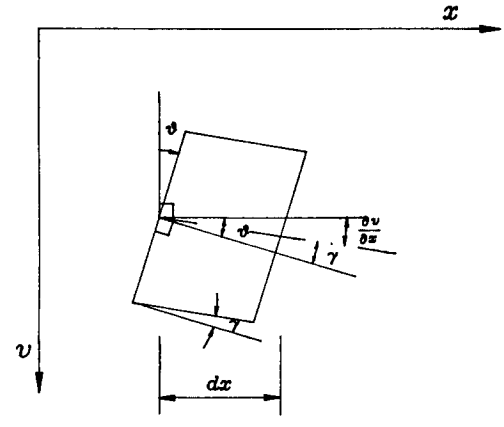

Fig. 2 Relation between deformed axis and rotated cross section.

2. Timoshenko beam theory

Consider a uniform cantilever of length l excited by support motion $v_g(t)$ and distributed loading $p(x, t)$ shown in Fig. 1. The transverse displacement of the beam relative to the clamped end is denoted $v(x, t)$. Let ρ be the mass density, E the Young's modulus, G the shear modulus, I the moment of inertia, A the cross-sectional area and A_s the effective shear area. Besides the transverse displacement v, Timoshenko theory requires another variable, the angle of rotation of the cross section $\theta(x, t)$. The relation between v and θ is shown in Fig. 2, which is expressed as

$$\frac{\partial v}{\partial x} = \theta - \gamma \tag{1}$$

in which γ is the angle of shear deformation. According to the following force-deformation relations for the moment M and the shear V

$$M = -EI\frac{\partial \theta}{\partial x} \tag{2}$$

$$V=-A_sG\left(\theta-\frac{\partial v}{\partial x}\right) \tag{3}$$

the equations of motion for the Timoshenko beam are expresses as

$$-A_sG\left(\frac{\partial\theta}{\partial x}-\frac{\partial^2 v}{\partial x^2}\right)-\rho A\frac{\partial^2 v}{\partial t^2}=-p+\rho A\frac{\partial^2 v_g}{\partial t^2} \tag{4}$$

$$EI\frac{\partial^2\theta}{\partial x^2}+A_sG\left(\frac{\partial v}{\partial x}-\theta\right)-\rho I\frac{\partial^2\theta}{\partial t^2}=0 \tag{5}$$

According to the normal-mode approach, v and θ are expressed as a linear combination of mode shapes,

$$v(x,\ t)=\sum_{n=1}^{\infty}\phi_n(x)\,Y_n(t) \tag{6}$$

$$\theta(x,\ t)=\sum_{n=1}^{\infty}\psi_n(x)\,Y_n(t) \tag{7}$$

in which Y_n is the amplitude of the nth mode, ϕ_n is the shape function corresponding to v and ψ_n is the shape function corresponding to θ. The frequency equation and the shape functions are derived by satisfying the following boundary conditions of the cantilever

$$v(0,\ t)=0;\qquad \theta(0,\ t)=0 \tag{8}$$

and

$$\frac{\partial\theta(l,\ t)}{\partial x}=0;\qquad \theta(l,\ t)-\frac{\partial v(l,\ t)}{\partial x}=0 \tag{9}$$

The frequency of the nth mode is calculated as

$$\omega_n=\frac{b_n}{l^2}\sqrt{\frac{EI}{\rho A}} \tag{10}$$

after solving the roots, b_n, from the frequency equation (Huang 1961)

$$2+[b_n{}^2(r^2-s^2)^2+2]\cosh b_n\alpha_n\cos b_n\beta_n-\frac{b_n(r^2+s^2)}{\sqrt{1-b_n{}^2r^2s^2}}\sinh b_n\alpha_n\sin b_n\beta_n=0 \tag{11}$$

in which

$$\alpha_n=\sqrt{\frac{-(r^2+s^2)+\sqrt{(r^2-s^2)^2+4/b_n{}^2}}{2}} \tag{12}$$

and

$$\beta_n=\sqrt{\frac{(r^2+s^2)+\sqrt{(r^2-s^2)^2+4/b_n{}^2}}{2}} \tag{13}$$

with

$$r=\frac{1}{l}\sqrt{\frac{I}{A}};\qquad s=\frac{1}{l}\sqrt{\frac{EI}{A_sG}} \tag{14}$$

The shape functions of the nth mode are

$$\phi_n(x)=C_1\left[\cosh b_n\alpha_n\frac{x}{l}-\frac{\alpha_n(\beta_n^2-s^2)}{\beta_n(\alpha_n^2+s^2)}\delta_n\sinh b_n\alpha_n\frac{x}{l}-\cos b_n\beta_n\frac{x}{l}+\delta_n\sin b_n\beta_n\frac{x}{l}\right] \tag{15}$$

and

$$\psi_n(x)=C_1\frac{b_n}{l}\frac{\beta_n^2-s^2}{\beta_n}\left[-\delta_n\cosh b_n\alpha_n\frac{x}{l}+\frac{\beta_n(\alpha_n^2+s^2)}{\alpha_n(\beta_n^2-s^2)}\sinh b_n\alpha_n\frac{x}{l}+\delta_n\cos b_n\beta_n\frac{x}{l}+\sin b_n\beta_n\frac{x}{l}\right] \tag{16}$$

in which

$$\delta_n=\frac{\frac{\beta_n}{\alpha_n}\sinh b_n\alpha_n-\sin b_n\beta_n}{\frac{\beta_n^2-s^2}{\alpha_n^2+s^2}\cosh b_n\alpha_n+\cos b_n\beta_n} \tag{17}$$

Because ϕ_n and ψ_n are not independent as defined in Eqs. (6) and (7), the same arbitrary constant C_1 is used in ϕ_n and ψ_n. The value of α_n is real only when $\sqrt{(r^2-s^2)^2+4/b_n^2}\geq(r^2+s^2)$, i.e., $b_n\leq 1/(rs)$. If $\sqrt{(r^2-s^2)^2+4/b_n^2}<(r^2+s^2)$, i.e., $b_n>1/(rs)$, α_n in Eq. (12) becomes imaginary; the shape functions in Eqs. (15) and (16) are still real except that the sin$h$ and cos$h$ terms become sin and cos. In the Bernoulli-Euler beam theory which does not take into account both rotatory inertia and transverse-shear deformation, $r=0$ and $s=0$ so that $\alpha_n=1/\sqrt{b_n}$ which is never imaginary and $\psi_n(x)=(\partial\phi_n(x))/(\partial x)$.

Substituting Eqs. (6) and (7) into Eqs. (4) and (5) and applying the following orthogonal property (Herrmann 1955)

$$\rho A\int_0^l(\phi_m\phi_n+\frac{I}{A}\psi_m\psi_n)\,dx=\begin{cases}M_n & \text{for } m=n\\ 0 & \text{for } m\neq n\end{cases} \tag{18}$$

in which M_n is the modal mass of the nth mode, the equations of motion in Eqs. (4) and (5) can be reduced to

$$\ddot{Y}_n(t)+\omega_n^2Y_n(t)=P_n(t) \tag{19}$$

in which

$$P_n(t)=\frac{\int_0^l p(x,\ t)\,\phi_n(x)\,dx-\rho A\ddot{v}_g(t)\int_0^l\phi_n(x)dx}{M_n} \tag{20}$$

and $(\dot{})$ represents differentiation with respect to time t.

3. Solution scheme

The model of a cantilever bouncing against a stop is shown in Fig. 3 in which the free end of the beam is separated by a gap d from an elastic stop which has stiffness k. The fixed end of the beam and the elastic stop are subjected to the same excitation of acceleration $\ddot{v}_g(t)$. When the displacement of the beam at the free end is larger than the gap, i.e., $v(l,\ t)>d$, the

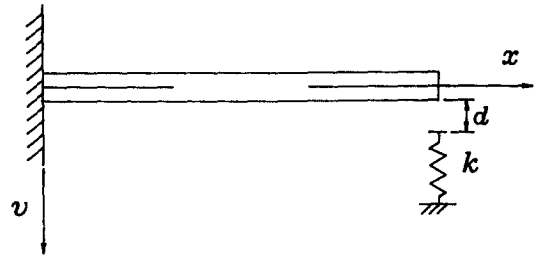

Fig. 3 Sketch of a cantilever with an elastic stop.

beam end makes contact with the elastic stop and is subject to a shear force that is equal to

$$N(t)=k[v(l,\ t)-d] \tag{21}$$

The vibration of the cantilever repeats two stages; one is the unconstrained stage in which the cantilever freely vibrates without touching the stop, and the other is the constrained stage in which the cantilever and the stop are in contact. Timoshenko beam theory is applied to solve this problem by defining the distributed loading as

$$p(x,\ t)=\begin{cases} -N(t)\,\delta(x-l) & \text{for } v(l,\ t)>d \\ 0 & \text{for } v(l,\ t)\leq d \end{cases} \tag{22}$$

in which $\delta(x-l)$ is the Dirac delta function.

When the free end makes contact with the stop, Eq. (19) becomes

$$\ddot{Y}_n(t)+\omega_n^2 Y_n(t)=f_n N(t)+g_n \ddot{v}_g(t) \tag{23}$$

in which

$$f_n=-\frac{\phi_n(l)}{M_n} \tag{24}$$

and

$$g_n=-\frac{\rho A\int_0^l \phi_n(x)\,dx}{M_n} \tag{25}$$

Eq. (23) can not be directly solved because the contact force $N(t)$ is unknown.

However, if the contact force is assumed to be linearly varied in time interval $\Delta=t_{i+1}-t_i$, Eq. (23) can be expressed as a form of the Duhamel integral equation and solved step-by-step by the so-called "piecewise-exact" method (Clough and Penzien 1993). The general solution at the time t_{i+1} has the forms as

$$Y_n(t_{i+1})=\frac{\dot{Y}_n(t_i)}{\omega_n}\sin\omega_n\Delta+Y_n(t_i)\cos\omega_n\Delta+N(t_i)f_n\left(\frac{\sin\omega_n\Delta}{\omega_n^3\Delta}-\frac{\cos\omega_n\Delta}{\omega_n^2}\right)+$$
$$N(t_{i+1})f_n\left(\frac{1}{\omega_n^2}-\frac{\sin\omega_n\Delta}{\omega_n^3\Delta}\right)+\frac{g_n}{\omega_n}\int_0^\Delta \ddot{v}_g(t_i+\tau)\sin\omega_n(\Delta-\tau)\,d\tau \tag{26}$$

and

$$\frac{\dot{Y}_n(t_{i+1})}{\omega_n}=\frac{\dot{Y}_n(t_i)}{\omega_n}\cos\omega_n\Delta-Y_n(t_i)\sin\omega_n\Delta+N(t_i)f_n\left(\frac{\sin\omega_n\Delta}{\omega_n^2}-\frac{1-\cos\omega_n\Delta}{\Delta\omega_n^3}\right)$$
$$+N(t_{i+1})f_n\left(\frac{1-\cos\omega_n\Delta}{\Delta\omega_n^3}\right)+\frac{g_n}{\omega_n}\int_0^{\Delta}\ddot{v}_g(t_i+\tau)\cos\omega_n(\Delta-\tau)\,d\tau \tag{27}$$

The contact force at the time t_{i+1} is found by substituting Eq. (26) into Eq. (6) and Eq. (21),

$$N(t_{i+1})=\left\{\sum_{n=1}^{\infty}\phi_n(l)\left[\frac{\dot{Y}_n(t_i)}{\omega_n}\sin\omega_n\Delta+Y_n(t_i)\cos\omega_n\Delta+N(t_i)f_n\left(\frac{\sin\omega_n\Delta}{\omega_n^3\Delta}-\frac{\cos\omega_n\Delta}{\omega_n^2}\right)+\right.\right.$$
$$\left.\left.\frac{g_n}{\omega_n}\int_0^{\Delta}\ddot{v}_g(t_i+\tau)\sin\omega_n(\Delta-\tau)\,d\tau\right]d\right\}\Big/\left[\frac{1}{k}-\sum_{n=1}^{\infty}\phi_n(l)f_n\left(\frac{1}{\omega_n^2}-\frac{\sin\omega_n\Delta}{\omega_n^3\Delta}\right)\right] \tag{28}$$

When the support motion $\ddot{v}_g(t)$ is specified, Eqs. (28), (26) and (27) form a set of recurrent equations to compute the response when the free end of the cantilever makes contact with the stop.

Because variation of contact force is assumed during an interval, accurate results are obtained only when the time interval applied in the calculation of contact force is small enough, but a small interval is inefficient when the cantilever is not in contact with the stop. Therefore, intervals of two kinds are adopted in a numerical calculation. A large interval is used in unconstrained stages whereas a small interval is used in constrained stages. The size of intervals depends on the stiffness ratio kl^3/EI. Higher value of the stiffness ratio has higher impact force and higher-frequency vibration so that smaller time interval is required.

4. Numerical examples

The model used in numerical simulation is an AISC steel section $W12\times53$; the dimensions defined in Fig. 4 are $h=0.3063$ m, $b_f=0.2539$ m, $t_f=0.0146$ m and $t_w=0.0088$ m. The cross-section area is $A=0.01006$ m^2 and the moment of inertial is $I=1.769\times10^{-4}$ m^4. The material properties are $\rho=8157$ kg/m^3, $E=2\times10^{11}$ N/m^2 and Poisson's ratio $\nu=0.3$. The corresponding shear modulus is $G=7.69\times10^{10}$ N/m^2 and the effective shear area is calculated (Cowper 1966) to be $A_s=2.416$

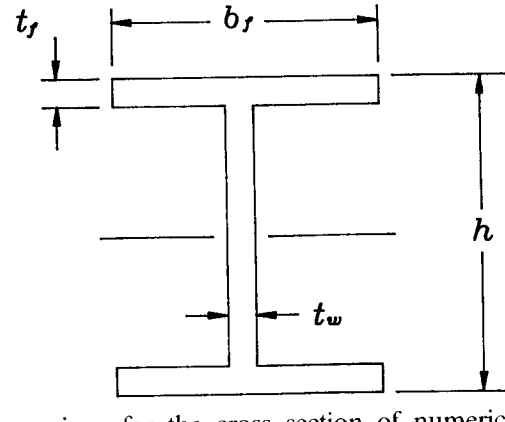

Fig. 4 Dimensions for the cross section of numerical example.

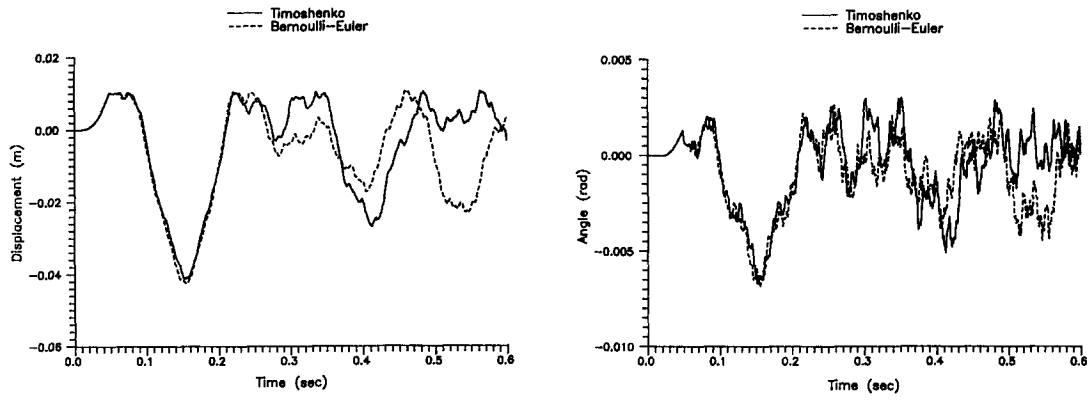

(a) Transverse displacement (b) Rotation of cross section

Fig. 5 Histories of transverse displacement and section rotation at the free end.

$\times 10^{-3}$ m^2. The length of the cantilever is $l=10$ m. The natural frequencies of the cantilever based on Timoshenko beam theory are 3.66, 22.3, 59.9, 111 and 173 Hz for the first five modes. If Bernoulli-Euler beam theory is applied, the corresponded frequencies are 3.67, 23.0, 64.5, 126 and 209 Hz, which shows that the Bernoulli-Euler beam is more rigid than the Timoshenko beam. The parameters defined in Eq. (14) are $r=0.01326$ and $s=0.04364$. The value of α_n becomes imaginary from the 27th mode of frequency 1828 Hz.

The stop has stiffness $k=1\times10^8$ N/m and the gap is $d=0.01$ m. The model is excited by a sinusoidal support acceleration $\ddot{v}_g=A\sin\omega_g t$ with which integration of $\ddot{v}_g$ in Eqs. (26), (28) and (27) is explicitly derived. The input acceleration is chosen to have amplitude $A=-10$ m/s^2 and frequency $\omega_g=8$ Hz. Since the stiffness ratio is high, $kl^3/EI=2826$, the interval used in the analysis is 10^{-4} *s* for unconstrained stages and 10^{-6} *s* for constrained stages. The solution may lose accuracy and not converge if shorter interval were used. In order to reduce the error created by mode truncation, 1000 modes were applied in modal combination for the Timoshenko beam model of which the period of the 1000 th mode is 1.734×10^{-5} *s*. For the Bernoulli-Euler beam model, 200 modes were applied of which the smallest period is 2.436×10^{-6} *s*.

The calculated histories of transverse displacement and rotational angle at the free end of the cantilever are plotted in Fig. 5. Also compared in this figure are the response histories of the Bernoulli-Euler beam, which indicates that the response difference between the two beam theories becomes obvious after some bounces of the cantilever. The contact force at the free end with the stop and the shear force at the fixed end are plotted in Fig. 6, which shows that the impact at the free end induces high-frequency shear force at the fixed end.

The contact force can be divided into many contact clusters. The contact force in the first contact cluster and the corresponding fixed-end shear of the Timoshenko beam are compared with those of the Bernoulli-Euler beam in Figs. 7(a) and 7(b), respectively. Although the beam makes contact with the stop at almost the same time according to both beam theories, the Bernoulli-Euler beam is more rapidly disturbed at the fixed end than the Timoshenko beam. Hence, the velocity of stress wave in the Bernoulli-Euler beam is greater than that in the Timoshenko beam. Figs. 7(c) and 7(d) put the contact force and the fixed-end shear together and show that the lag between the contact force and the fixed-end shear is about 0.005 *s* for the Timoshenko beam and 0.001 *s* for the Bernoulli-Euler beam.

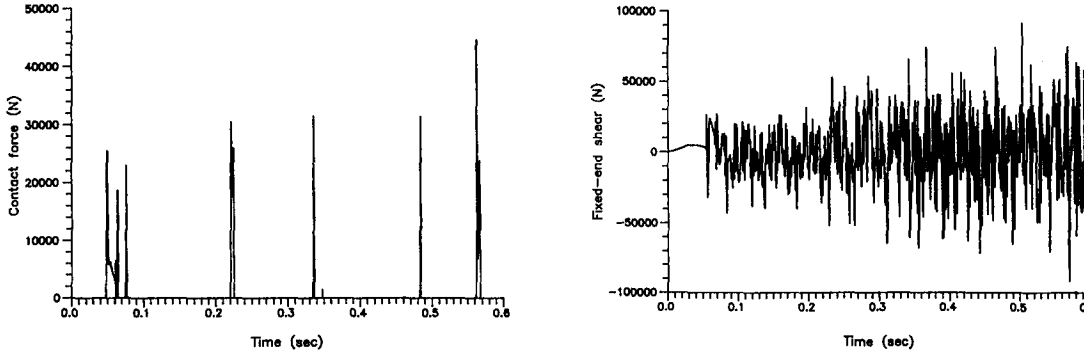

(a) Contact force (b) Fixed-end shear

Fig. 6 Histories of contact force at the free end and shear force at the fixed end of Timoshenko beam.

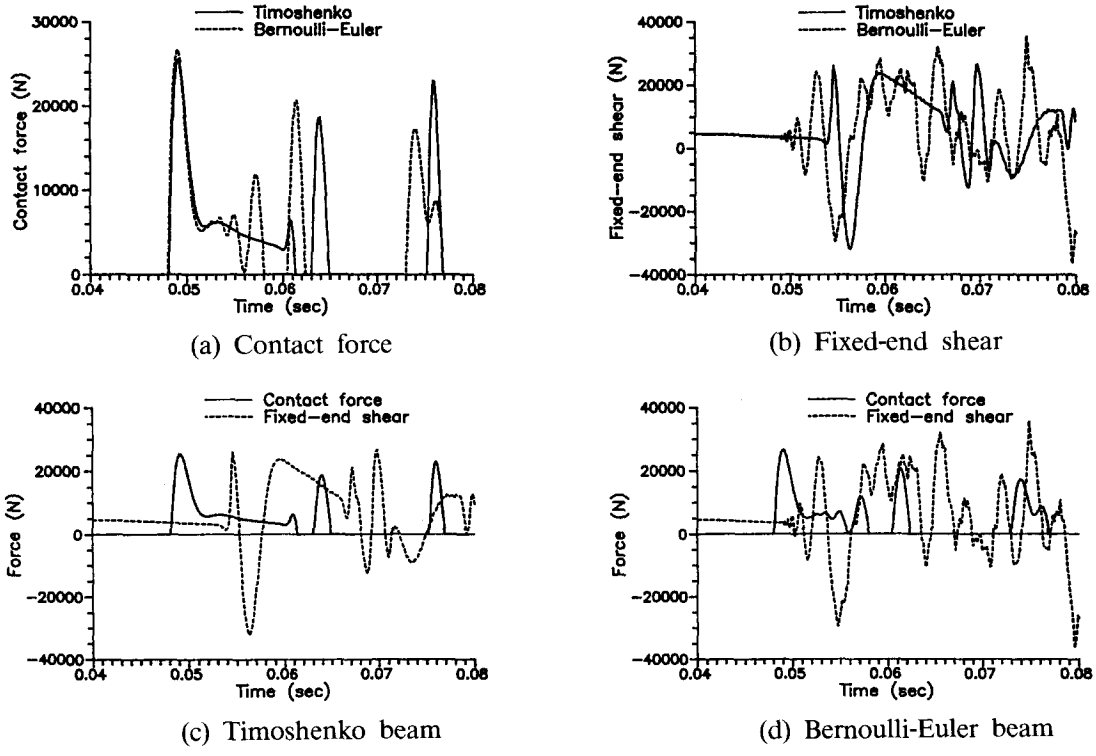

(a) Contact force (b) Fixed-end shear

(c) Timoshenko beam (d) Bernoulli-Euler beam

Fig. 7 Comparison of contact force and fixed-end shear between Timoshenko beam and Bernoulli-Euler beam.

The distribution of shear force along the Timoshenko beam axis at four points of time during the first contact cluster are plotted in Fig. 8, which shows the traveling of force peaks. To provide a better view of wave propagation, the variation of the distribution of shear force with time during the first contact cluster is shown in Fig. 9(a), which is the projection of a three-dimensional drawing. The beam axis is perpendicular to the time axis, of which the free end is at the top of the figure and the fixed end at the bottom. The shear force is plotted in the third direction.

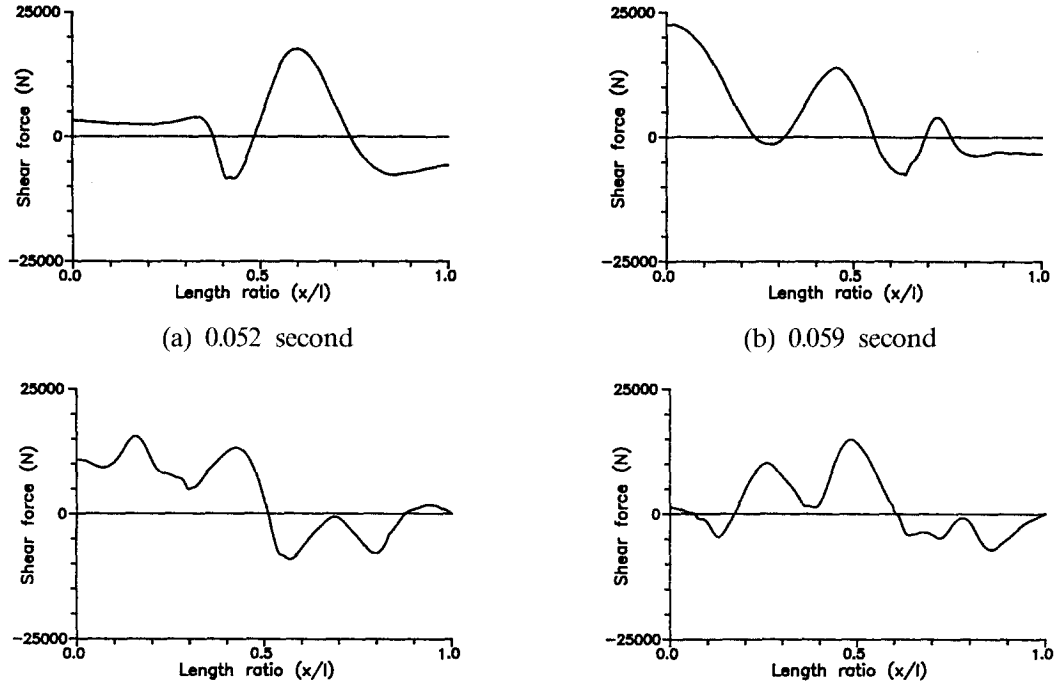

(a) 0.052 second (b) 0.059 second

(c) 0.066 second (d) 0.072 second

Fig. 8 Shear force distribution of Timoshenko beam at four points of time during the first contact cluster.

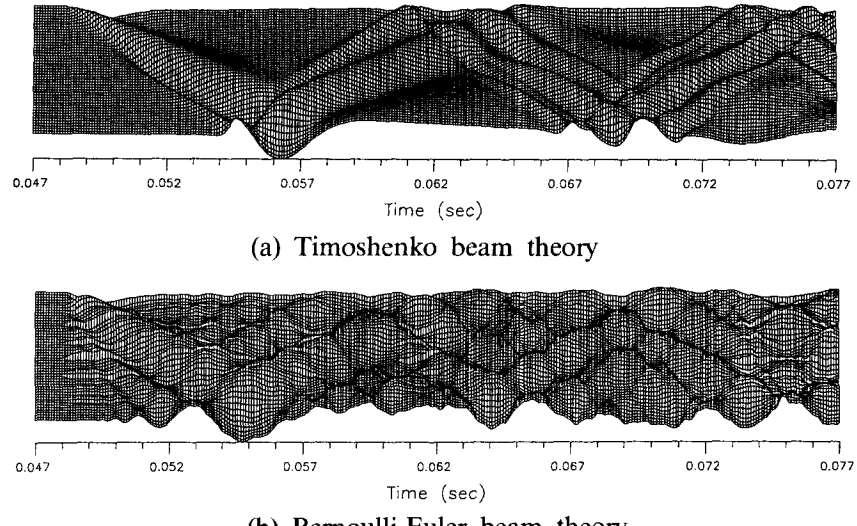

(a) Timoshenko beam theory

(b) Bernoulli-Euler beam theory

Fig. 9 Variation of shear force distribution with time during the first contact cluster.

In this figure, each ridge represents the traveling of a force peak. There are some saddles near the free end and the fixed end, because of interference of incoming waves and reflecting waves. Fig. 9(b) shows the variation of the Bernoulli-Euler beam, which indicates more saddles occurred

because the faster wave velocity generates more interference.

5. Conclusions

A method based on Timoshenko beam theory to calculate the support-excited vibration of a cantilever of which the free end is separated by a gap froman elastic stop was proposed. Although the response was a non-linear boundary condition problem, the proposed method treated the contact force applied by the stop on the cantilever as an external force and assumed the contact force linearly varied in a time interval, so that the classical mode approach could be employed to solve the response.

The effects of rotatory inertia and shear deformation on the bouncing behavior of the cantilever against the stop were addressed in a numerical example. The wave velocity of shear force in the Timoshenko beam was less than that in the Bernoulli-Euler beam; thus the patterns of deformation and shear distribution during bouncing of the cantilever made a large difference between the Timoshenko beam and Bernoulli-Euler beam.

Acknowledgements

The research work reported in this paper was supported by the National Science Council, Republic of China, under Grant No. NSC 83-0410-E011-022. This support is greatly appreciated.

References

Aprahamian, R. and Evensen, D.A. (1970) "Applications of holography to dynamics: high-frequency vibrations of beams", *Journal of Applied Mechanics ASME*, **37**, 287-291.

Clough, R.W. and Penzien, J. (1993) *Dynamics of Structures*, 2nd edition, McGraw-Hill, Singapore.

Cowper, G.R. (1966) "The shear coefficient in Timoshenko's beam theory", *Journal of Applied Mechanics ASME*, **33**, 335-340.

Herrmann, G. (1955) "Forced motions of Timoshenko beams", *Journal of Applied Mechanics ASME*, **22**, 53-56.

Huang, T.C. (1961) "The effect of rotatory inertia and of shear deformation on the frequency and normal mode equations of uniform beams with simple end conditions", *Journal of Applied Mechanics ASME*, **28**, 579-584.

Kelly, J.M. (1967) "The impact of a mass on a beam", *International Journal of Solids and Structures*, **3**, 191-196.

Lo, C.C. (1980) "A cantilever beam chattering against a stop", *Journal of Sound and Vibration*, **69**, 245-255.

Maison, B.F. and Kasai, K. (1990) "Analysis for type of structural pounding", *Journal of Structural Engineering ASCE*, **116**, 957-977.

Masri, S.F., Mariamy, Y.A. and Anderson, J.C. (1981) "Dynamic response of a beam with a geometric nonlinearity", *Journal of Applied Mechanics ASME*, **48**, 404-410.

Salmon, M.A., Verma, V.K. and Youtsos, T.G. (1985) "Elastic analysis of beam-support impact", *Journal of Pressure Vessel Technology ASME*, **107**, 64-67.

Shaw, S.W. (1985) "Forced vibrations of a beam with one-side amplitude constraint:theory and experiment", *Journal of Sound and Vibration*, **99**, 199-212.

Tsai, H.-C., Lin, C.-W. and Tang, Y.K. (1989) "Response spectrum analysis of multiple support excitation on piping system with gapped supports", *ASME Pressure Vessel and Piping Conference*, Honolulu, PVP-182, 317-324.